Liquid Crystals
Publication details, including instructions for authors and subscription information:
http://www.informaworld.com/smpp/title~content=t713926090

Critical heat capacity at nematic-smectic A_1 and smectic A_1-smectic A_2 transitions in DB_5CN TBBA

P. Das[a]; G. Nounesis[a]; C. W. Garland[a]; G. Sigaud[b]; Nguyen Huu Tinh[b]
[a] Department of Chemistry and Center for Material Science and Engineering, Massachusetts Institute of Technology, Cambridge, Massachusetts, U.S.A. [b] Centre de Recherche Paul Pascal, Domaine Universitaire, Talence, France

To cite this Article Das, P. , Nounesis, G. , Garland, C. W. , Sigaud, G. and Tinh, Nguyen Huu(1990) 'Critical heat capacity at nematic-smectic A_1 and smectic A_1-smectic A_2 transitions in DB_5CN TBBA', Liquid Crystals, 7: 6, 883 — 893
To link to this Article: DOI: 10.1080/02678299008033846
URL: http://dx.doi.org/10.1080/02678299008033846

LIQUID CRYSTALS, 1990, VOL. 7, NO. 6, 883–893

Critical heat capacity at nematic–smectic A_1 and smectic A_1–smectic A_2 transitions in DB_5CN + TBBA

by P. DAS†, G. NOUNESIS and C. W. GARLAND
Department of Chemistry and Center for Material Science and Engineering, Massachusetts Institute of Technology, Cambridge, Massachusetts 02139, U.S.A.
G. SIGAUD and NGUYEN HUU TINH
Centre de Recherche Paul Pascal, Domaine Universitaire, 33405 Talence, France

(*Received 18 October 1989; accepted 18 January 1990*)

High-resolution heat capacity measurements have been made on mixtures of pentylphenylcyanobenzoyloxy benzoate (DB_5CN) and terephthal-bis-butylaniline (TBBA). These mixtures exhibit a nematic (N)–smectic A_1 (S_{A_1})–smectic A_2 (S_{A_2}) phase sequence. Detailed N–S_{A_1} data were obtained on one mixture and are in good agreement with the 3D-XY model, which is known to provide an excellent description of the critical N–S_{A_1} heat capacity in other systems. The S_{A_1}–S_{A_2} heat capacity for all the investigated mixtures exhibits a finite cusp. The critical exponents for these heat capacity peaks are consistent with the Fisher–renormalized Ising value $\alpha_R = -0{\cdot}124$, but the experimental situation may be more complex. The magnitude of the $C_p(A_1$–$A_2)$ peaks decreases markedly as X increases.

1. Introduction

Polar liquid crystals with three-ring aromatic cores exhibit a wide variety of smectic polymorphism [1]. Mixtures of 4-*n*-alkylphenyl-4′-4″-cyanobenzoyloxy benzoate, DB_nCN, and terephthal-bis-4-*n*-butylaniline, TBBA, are of special interest since they exhibit the phase sequence N–S_{A_1}–S_{A_2} [1, 2]. N denotes the nematic phase, S_{A_1} the monolayer smectic A phase (with layer thickness $d = L$, where L is the molecular length), and S_{A_2} the bilayer smectic A (with $d = 2L$). Note that the nonpolar TBBA has a molecular length almost equal to that of DB_6CN. Very similar phase diagrams are observed for DB_5CN + TBBA, DB_6CN + TBBA, and DB_7CN + TBBA [1–3]. In each case, there is a direct S_{A_1}–S_{A_2} transition without intervening modulated phases such as the fluid antiphase $S_{\tilde{A}}$ and the crenelated phase $S_{A_{cren}}$ seen in other binary mixtures involving DB_nCN [4].

The phase topology in DB_nCN + TBBA mixtures predicted using the phenomenological frustrated-smectics model of Prost [5] is in good agreement with experiment. Figure 1 shows the relevant part of the DB_5CN + TBBA phase diagram. There is a N–S_{A_1}–S_{A_2} 'triple point' at a TBBA concentration X^*. For $X < X^*$, the direct N–S_{A_2} transition is first order. The S_{A_1}–S_{A_2} transition is predicted to be second order in general but to exhibit a tricritical point at X_t near X^* (and weak first-order character between X^* and X_t). The N–S_{A_1} transition is predicted to be second order for all $X > X^*$. Thus, the 'triple point' is a N–S_{A_1} critical endpoint in the Prost model. These theoretical features have been generally confirmed by studies of DB_6CN + TBBA mixtures [3, 6].

† Present address: 7C Kali Charan Sett Lane, Calcutta 700030, India.

0267–8292/90 $3.00

The only high-resolution studies of critical behaviour near a S_{A_1}–S_{A_2} transition have been on the binary mixture DB_6CN + TBBA. An X-ray study has been made of the order-parameter susceptibility and the correlation lengths parallel and perpendicular to the director for several TBBA concentrations [3]. The S_{A_1}–S_{A_2} line exhibits a tricritical point at $X_t \simeq 0{\cdot}121$ very close to $X^* \simeq 0{\cdot}117$. The critical exponents γ, $\nu_\parallel$ and $\nu_\perp$ are invariant along the second-order part of the S_{A_1}–S_{A_2} line and the correlation length exponents are isotropic: $\gamma = 1{\cdot}46 \pm 0{\cdot}05$, $\nu_\parallel = \nu_\perp = 0{\cdot}74 \pm 0{\cdot}03$. Surprisingly, these numbers also seem to be valid near the tricritical point where the transition turns first order. One mixture, DB_6CN + 15 mol % TBBA, has also been investigated calorimetrically and the critical exponent α is $-0{\cdot}15 \pm 0{\cdot}06$ [7]. These exponent values satisfy the hyperscaling relation $\alpha + 3\nu = 2$ within experimental error (α exp + 3ν exp = $2{\cdot}07 \pm 0{\cdot}15$), but the negative α value indicates a finite cusp in C_p rather than a divergent power-law singularity.

Both the mean-field frustrated smectics model [5] and a renormalization group model [8] that includes fluctuation effects place the S_{A_1}–S_{A_2} transition in the 3D Ising universality class. Since the Ising critical exponents are $\gamma_I = 1{\cdot}24$, $\nu_I = 0{\cdot}63$, and $\alpha_I = 0{\cdot}11$ [9], it is clear that the experimental exponents do not have the expected Ising values. This apparent disagreement has been explained in terms of Fisher renormalization of the critical behaviour [10]. As pointed out by Huse [11], the theoretical Ising exponents describe the critical behaviour at constant chemical potential whereas the measurements are made at constant mole fraction X. For sufficiently large values of $(dT_c/dX)^2$, i.e. for steep phase boundaries, Fisher renormalized exponents may be observed [11, 12]

$$2 - \alpha_R = (2 - \alpha)/(1 - \alpha), \quad \nu_R = \nu/(1 - \alpha), \quad \gamma_R = \gamma/(1 - \alpha). \qquad (1)$$

The Fisher–renormalized Ising values are $\alpha_R = -0{\cdot}124$, $\nu_R = 0{\cdot}71$, and $\gamma_R = 1{\cdot}39$, which agree fairly well with the experimental DB_6CN + TBBA values.

The present investigation is concerned with a high-resolution calorimetric study of seven DB_5CN + TBBA mixtures, with emphasis on the S_{A_1}–S_{A_2} transition. The principal goals are to clarify the role of Fisher renormalization, to explore the question of a S_{A_1}–S_{A_2} tricritical point, and to determine how the magnitude of the excess heat capacity varies along the S_{A_1}–S_{A_2} line. In addition, a high-resolution study of the N–S_{A_1} transition was carried out on one of the mixtures, and the direct first-order N–S_{A_2} transition was observed in another mixture.

2. Results and analysis

The compositions and transition temperatures for the investigated DB_5CN + TBBA mixtures are given in table 1. The compound DB_5CN was synthesized and purified at the Centre de Recherche Paul Pascal. The TBBA was a commercial product (obtained from CPAC-Organix) that was recrystallized several times from ethanol and vacuum dried. High initial purity for the pure compounds and very careful handling are crucial for success. During the preparation of mixtures and the filling of the calorimeter cell, the materials were handled in vacuum or in oxygen-free, moisture-free atmospheres of argon or dry nitrogen. A silver sample cell containing ~ 80 mg of liquid crystal mixture was hermetically sealed with a cold-welded tin seal.

The heat capacity was measured using a microcomputer-controlled AC calorimeter described elsewhere [13]. This calorimeter operates at a constant frequency $\omega = 0{\cdot}196$,

Table 1. Transition temperatures and S_{A_1}–S_{A_2} integrated transition enthalpy δH for mixtures of DB_5CN + TBBA. The mole fraction of TBBA is denoted by X. Enthalpy values are given in units of $J\,g^{-1}$. Smooth curve values of the slope $dT_{A_1A_2}/dX$ are also given in units of K.

X	T_{NA_1}/K	$T_{A_1A_2}$/K	$-dT_{A_1A_2}/dX$	$\delta H(A_1$–$A_2)$
0·087	400·5†			>4
0·106	401·25	397·67	125	4·0
0·1214	–	395·04	110	3·63
0·134	403·15	393·1	110	3·42
0·1528	404·75	393·05	135	2·53
0·163	405·36	391·77	155	2·43
0·189	408·3	383·45	345	1·2

† This is a direct N–S_{A_2} transition temperature.

and the sample cell undergoes zero-to-peak temperature oscillations of ~5 mK. The temperature was typically scanned at a rate of 70 mK/h. The specific heat capacity was determined from

$$C_p = [C_p(\text{obs}) - C_p(\text{empty})]/m, \tag{2}$$

where C_p(obs) is the observed heat capacity of the filled cell (typically $0{\cdot}35\,J\,K^{-1}$), C_p(empty) is the heat capacity of the empty cell, which varied linearly from $\sim 0{\cdot}144\,J\,K^{-1}$ at 380 K to $\sim 0{\cdot}145\,J\,K^{-1}$ at 405 K, and m is the sample mass in grams. The S_{A_1}–S_{A_2} transition temperatures were quite stable: drift rates $-dT_c/dt$ were less than 1 mK/h except for the sample with $X = 0{\cdot}1214$, where $-dT_c/dt = 2$ mK/h. The N–S_{A_1} transition temperatures were much less stable: $-dT_c/dt \simeq 10$ mK/h except for the sample with $X = 0{\cdot}163$ (for which it was 5 mK/h). A detailed high-resolution study of the N–S_{A_1} transition was carried out only for the $X = 0{\cdot}163$ sample. In the other mixtures, the N–S_{A_1} C_p peak was determined with medium resolution in order to provide a C_p (baseline) curve for use in the analysis of the S_{A_1}–S_{A_2} transition.

As shown in figure 1, the phase diagram determined in this investigation is shifted slightly with respect to the diagram reported previously [2]. The main differences are (1) higher transition temperatures and (2) the S_{A_1} phase first appears at a smaller value of X_{TBBA}. We attribute these differences to higher chemical purity for the present mixtures, especially a better quality TBBA. The melting point for the crystal phase (CrK) lies in the range 393–395 K for these mixtures. Thus several of the S_{A_1}–S_{A_2} transitions are monotropic. Freezing of the S_{A_2} phase usually occurred in the range 378–382 K, well below the S_{A_1}–S_{A_2} transition except for the $X = 0{\cdot}189$ sample. In the latter mixture, a fast scan rate (850 mK/h) was used to prevent freezing from interfering with the S_{A_1}–S_{A_2} transition.

The heat capacity variation for the $X = 0{\cdot}087$ sample is shown in figure 2. The N–S_{A_2} transition is quite strongly first order, and data points obtained in the 1·9 K wide two-phase coexistence region are not true C_p values. These points are indicated by crosses. Figure 2 also shows anomalous effects in the CrK phase just below the first-order freezing of the S_{A_2} phase.

An overview of the C_p variations associated with the N–S_{A_1} and S_{A_1}–S_{A_2} transitions is given in figure 3. Data for the $X = 0{\cdot}1214$ sample are omitted here in order to improve the clarity of the display and because no reliable N–S_{A_1} data are available for

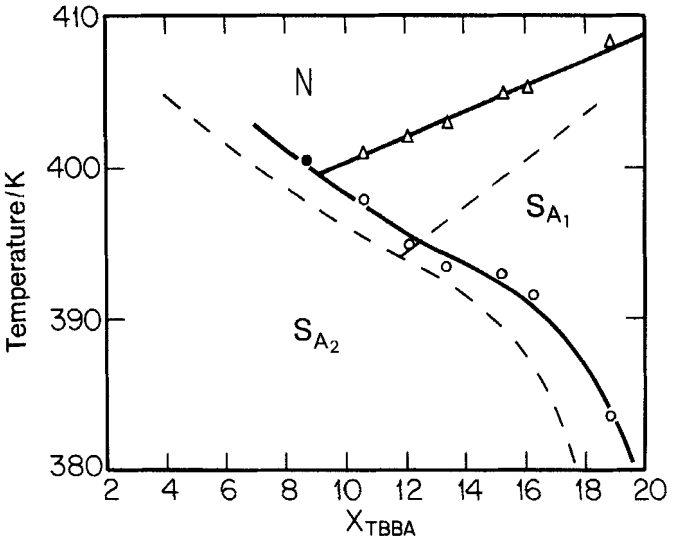

Figure 1. Partial phase diagram for binary mixtures of DB_5CN + TBBA. The phase transition lines reported in [2] are given as dashed curves. X is the mole fraction of TBBA, and the solid point denotes the direct first-order $N-S_{A_2}$ transition observed for $X = 0{\cdot}087$.

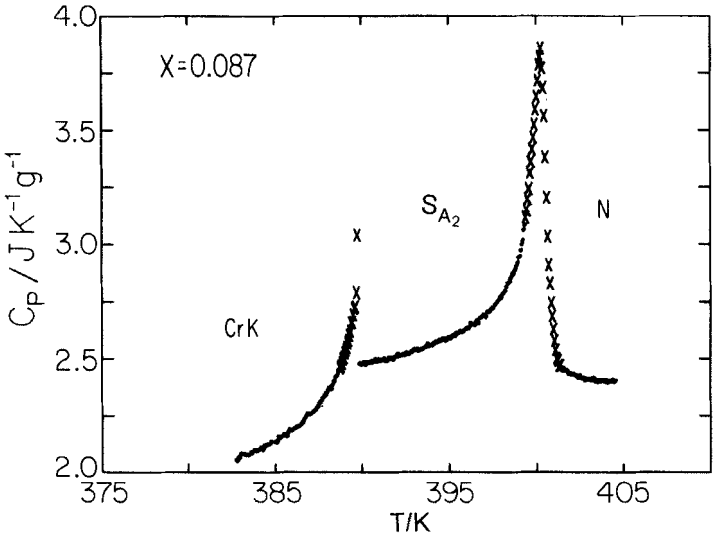

Figure 2. Heat capacity for a DB_5CN + TBBA mixture containing 8·70 mole % TBBA. Data points obtained in two-phase coexistence regions are denoted by crosses. The $S_{A_2} \rightarrow$ CrK freezing temperature on cooling varied somewhat from run to run for this sample and the other mixtures studied.

that composition. The $S_{A_1}-S_{A_2}$ peak for $X = 0{\cdot}1214$ is very similar to that observed for $X = 0{\cdot}106$ (see figure 5). The dashed lines represent C_p (baseline) curves determined in the manner described below.

The data for the $X = 0{\cdot}134$ mixture are the least reliable of those shown. The position of the $S_{A_1}-S_{A_2}$ peak was stable, but the peak was rounded and varied somewhat in size from run to run. The qualitative features of $C_p(T)$ agree well with

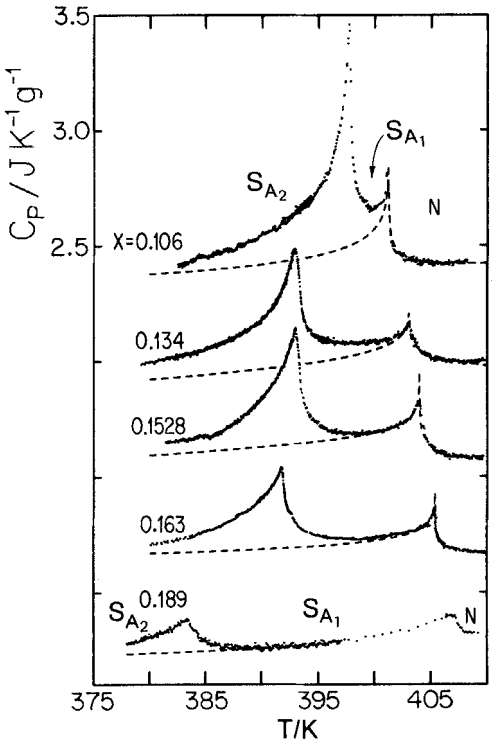

Figure 3. Overview of the C_p variation associated with N–S_{A_1} and S_{A_1}–S_{A_2} transitions in five mixtures of DB_5CN + TBBA. X denotes the mole fraction of TBBA. Each successive data set has been shifted down by 0·35 J K^{-1} g^{-1} relative to the preceding set (i.e. the X = 0·189 data are shifted down by 1·40 J K^{-1} g^{-1} relative to the unshifted X = 0·106 data). The dashed lines represent the baseline curves used in the analysis of the S_{A_1}–S_{A_2} critical heat capacity. These lines are the low-temperature tails of the N–S_{A_1} transition peaks (see figure 4 and text).

those for other samples, but these data are not of sufficient quality to merit detailed analysis.

The heat capacity data have been analysed using the renormalization group expression

$$C_p = A^{\pm}|t|^{-\alpha}(1 + D^{\pm}|t|^{\Delta_1} + \cdots) + B + E\Delta T, \quad (3)$$

where $t \equiv (T - T_c)/T_c$ is the reduced temperature and $\pm$ indicates above and below T_c. The corrections-to-scaling exponent Δ_1 is 0·5. The quantity B consists of both a regular contribution B_r and a critical contribution B_c, and the regular term $E\Delta T = E(T - T_c)$ represents the noncritical temperature dependence of C_p. When there are two overlapping critical heat capacity peaks, as in the present case, it is necessary to decompose the heat capacity into three components. We have done this using the simplifying assumption that $C_p = C_p$(background) + ΔC_p(N–A_1) + ΔC_p(A_1–A_2), where C_p (background) = $B_r + E\Delta T$ and ΔC_p is an excess critical heat capacity given by

$$\Delta C_p = A^{\pm}|t|^{-\alpha}(1 + D^{\pm}|t|^{0.5}) + B_c. \quad (4)$$

The analysis will be illustrated by a detailed description of the treatment of the X = 0·163 sample; see figure 4. The first step is the analysis of data close to T_{NA_1},

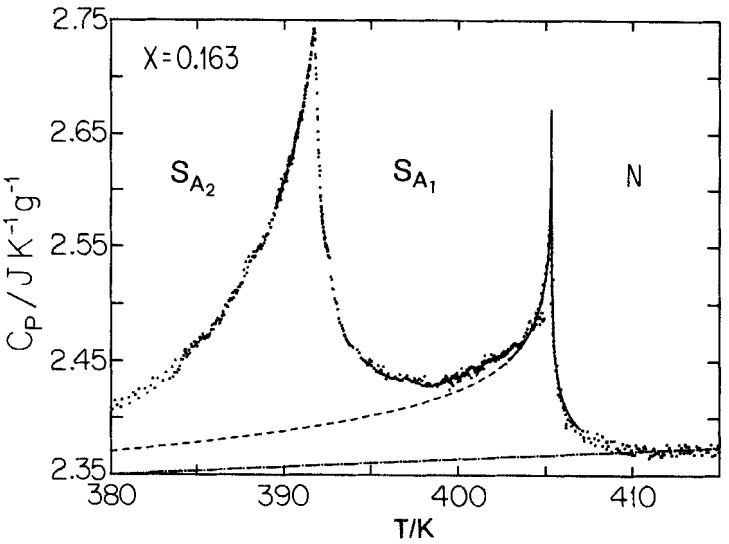

Figure 4. Specific heat of DB_5CN + 16·30 mole% TBBA. The dot–dash line shows the linear C_p (background) variation, which has a slope of 0·0007 J K^{-2}g^{-1}. A least-squares fit to the N–S_{A_1} peak over the range $|T - T_{NA_1}| \leqslant 2$ K is shown by the solid line (see text). The dashed curve labelled C_p(N–A_1) indicates the estimated C_p (baseline) for the S_{A_1}–S_{A_2} peak formed by the tail of the N–S_{A_1} peak. This dashed curve, which is an extrapolation of the N–S_{A_1} fitting curve, has a slope of 0·0023 J K^{-2}g^{-1} at $T_{A_1A_2}$.

where the contribution of $\Delta C_p(A_1\text{–}A_2)$ can be neglected. The solid curve over the range $|T - T_{NA_1}| \leqslant 2$ K in figure 4 represents a fit to the N–S_{A_1} peak with equation (3). When the N–S_{A_1} exponent α was allowed to be a free parameter in a least-squares fit with $D^+ = D^- = 0$ fixed, the resulting parameter values were $\alpha = 0{\cdot}0063$, $A^+ = 5{\cdot}301$ J K^{-1}g^{-1}, $A^-/A^+ = 1{\cdot}014$, $B = -5{\cdot}467$ J K^{-1}g^{-1}, $E = 0{\cdot}0001$ J K^{-2}g^{-1} and $T_c = 405{\cdot}31$ K, with $\chi^2_\nu = 1{\cdot}32$. Note that α is close to the theoretically expected 3D-XY value of $-0{\cdot}007$ [9]. Furthermore, several high-resolution studies of very stable N–S_{A_1} transitions yield α_{exp} values equal to α_{XY} [14]. Thus we have tested a fit to this N–S_{A_1} peak with α fixed at $-0{\cdot}007$. The resulting parameter values are $A^+ = -5{\cdot}883$ J K^{-1}g^{-1}, $A^-/A^+ = 0{\cdot}983$, $D^+ = -0{\cdot}0803$, $D^-/D^+ = 0{\cdot}342$, $B = 8{\cdot}021$ J K^{-1}g^{-1}, ($B_r = 2{\cdot}368$ and $B_c = 5{\cdot}653$), $E = 0{\cdot}0007$ J K^{-2}g^{-1} and $T_c = 405{\cdot}361$ K, with $\chi^2_\nu = 1{\cdot}22$. This fit is statistically equivalent to the free α fit and the A^-/A^+ ratio agrees well with value 0·99 established for other N–S_{A_1} transitions [14]. Furthermore, the dimensionless ratio $R^+ \equiv A^+|D^+|^{\alpha/\Delta_1}/B_c$ equals $-1{\cdot}078$, in good agreement with its universal theoretical value ($-1{\cdot}057 \pm 0{\cdot}022$) and experimental value in other N–S_{A_1} systems ($-1{\cdot}073 \pm 0{\cdot}03$) [14]. This XY fit is shown in figure 4, and the dashed line represents an extrapolated low temperature tail of the N–S_{A_1} fit.

The next step in the analysis is to determine $\Delta C_p(A_1\text{–}A_2)$, the excess heat capacity associated with the S_{A_1}–S_{A_2} transition

$$\Delta C_p(A_1\text{–}A_2) = C_p - C_p(N\text{–}A_1), \tag{5}$$

where C_p(N–A_1) is represented by the dashed line in figure 4, as discussed above. Similar C_p(N–A_1) baseline curves were chosen for all of the mixtures (see figure 3). These curves were generated by fitting each N–S_{A_1} peak over a narrow temperature

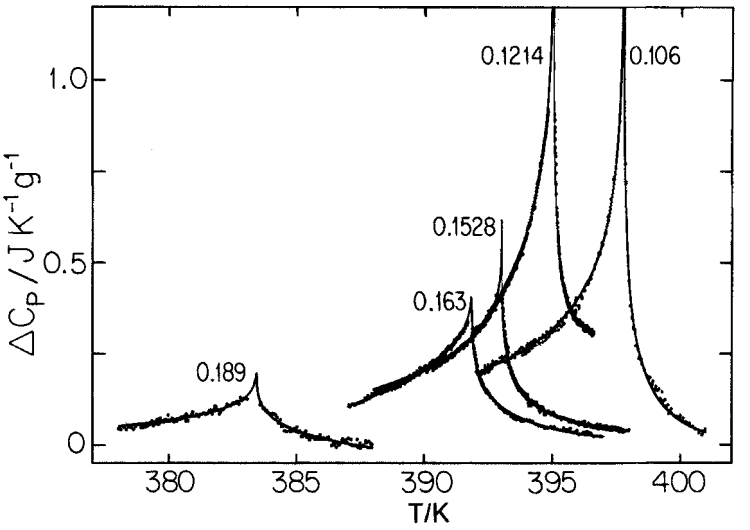

Figure 5. Least-squares fits to the excess heat capacity $\Delta C_p(A_1\text{–}A_2)$ for five mixtures of DB_5CN + TBBA. The parameter values are listed in table 2. The fits shown here are type I fits (α free).

range with equation (3) holding $\alpha = -0{\cdot}007$ and $A^-/A^+ = 0{\cdot}983$ fixed and then extrapolating the resulting fit down to ~ 380 K. The excess $\Delta C_p(A_1\text{–}A_2)$ curves obtained using these baseline curves are shown in figure 5 and will be analysed with equation (4). In the case of the sample with $X = 0{\cdot}1214$, the $C_p(N\text{–}A_1)$ baseline curve was estimated by using the parameters $A^{\pm}$, $D^{\pm}$ and E obtained for $X = 0{\cdot}106$, a $N\text{–}S_{A_1}$ transition temperature taken from the phase diagram, and a B value chosen so that the $\Delta C_p(A_1\text{–}A_2)$ excess peak fit in with the others in figure 5.

The various $\Delta C_p(A_1\text{–}A_2)$ curves were fit with equation (4) over the reduced temperature range $t_{min} < |t| < t_{max}$. t_{max} was $7{\cdot}5 \times 10^{-3}$ for the $X = 0{\cdot}106$ mixture, 4×10^{-3} for the $X = 0{\cdot}1214$ mixture and 10^{-2} for all the others. Because of extensive

Table 2. Least-squares parameters for fitting $\Delta C_p(A_1\text{–}A_2)$ with equations (4). The units for A^+ and B are J K^{-1} g^{-1}. Two types of fits are presented. For type I fits, the critical exponent α was a freely adjustable parameter. For type II fits, α was held fixed at the Fisher–renormalized Ising value $\alpha_R = -0{\cdot}124$.

X	Fit type	α	A^+	A^-/A^+	D^+	D^-	B_c	T_c/K	χ^2_ν
0·106	I	−0·032	−10·027	0·945	−0·482	−0·214	8·273	397·767	2·04
	II	−0·124	−5·801	0·820	−1·997	−1·014	2·673	397·755	3·72
0·1214	I	−0·091	−5·863	0·810	−2·364	−0·121	3·338	395·040	1·44
	II	−0·124	−5·821	0·758	−3·178	−0·302	2·675	395·038	1·48
0·1528	I	−0·173	−1·784	0·625	−1·751	0·562	0·709	393·024	1·32
	II	−0·124	−1·614	0·717	−1·007	0·447	0·867	393·024	1·63
0·163	I	−0·205	−1·471	0·513	−1·699	2·890	0·509	391·840	0·75
	II	−0·124	−1·034	0·625	0·042	3·119	0·614	391·850	1·05
0·189	I	−0·161	−0·612	0·778	0	0	0·291	383·445	2·04
	II	−0·124	−0·630	0·821	0	0	0·357	383·454	2·04

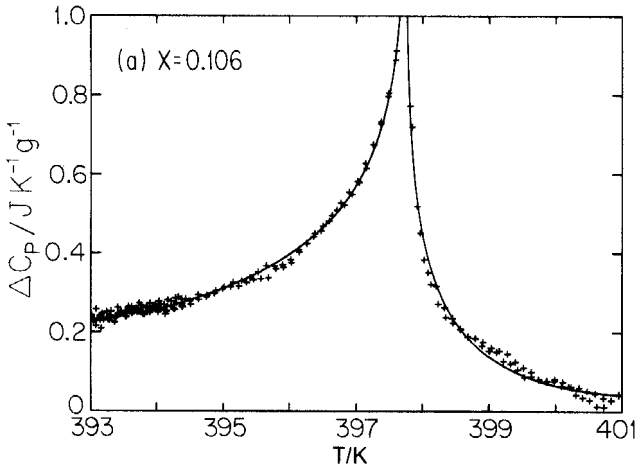

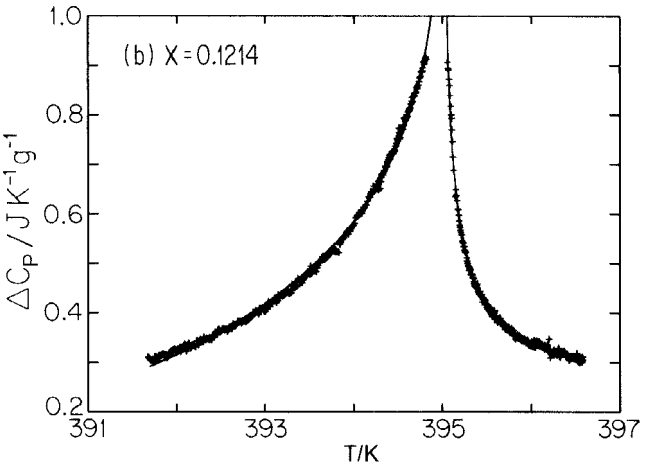

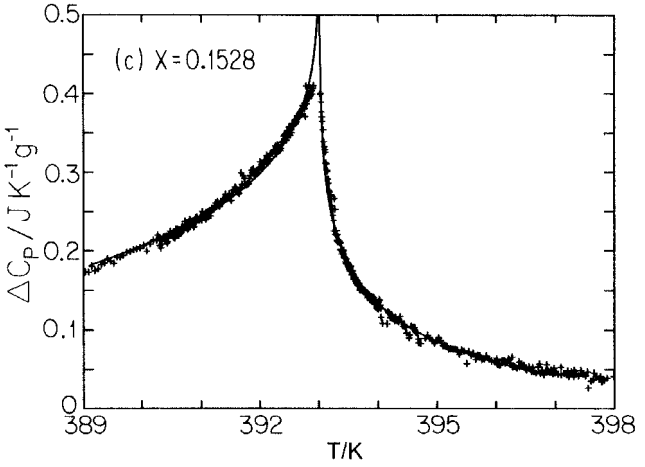

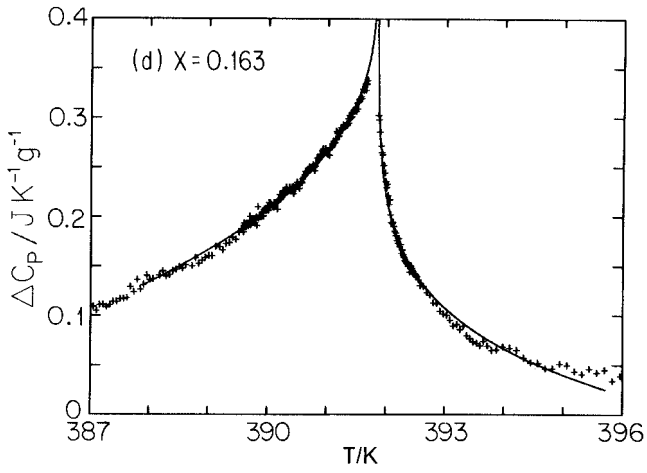

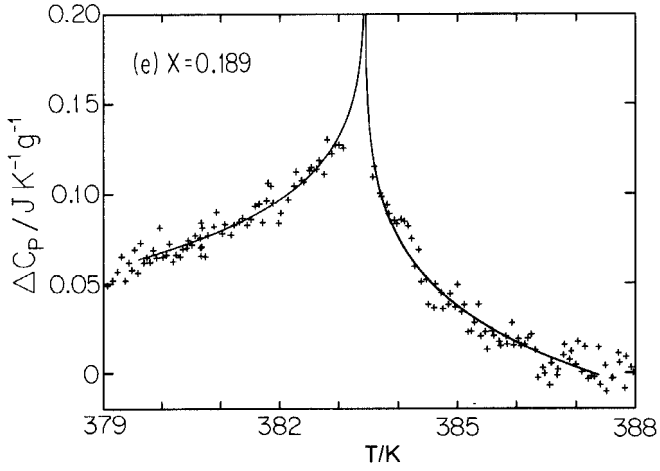

Figure 6. Least-squares fits (type II) to the excess heat capacity for (*a*) $X = 0{\cdot}106$, (*b*) $X = 0{\cdot}1214$, (*c*) $X = 0{\cdot}1528$, (*d*) $X = 0{\cdot}163$, and (*e*) $X = 0{\cdot}189$ mixtures.

rounding near T_c, the t_{min} values are quite large. They vary between $1{\cdot}6 \times 10^{-4}$ and $1{\cdot}9 \times 10^{-4}$ for all the mixtures except $X = 0{\cdot}189$ for which $t_{min} = 6{\cdot}4 \times 10^{-4}$. In table 2 the least-squares parameter values are given for two types of fits. For type I fits the critical exponent α was a free parameter, while for type II fits the value of α was held fixed at $-0{\cdot}124$, which is the Fisher renormalized α value for the 3D Ising universality class. In the case of the $X = 0{\cdot}189$ mixture, the corrections-to-scaling terms in equation (4) were set equal to zero. Since $\Delta C_p(A_1\text{–}A_2)$ is small for this mixture, the scatter in the data is fairly large, and extensive rounding occurs near T_c, these $D^{\pm}$ terms were found to be statistically insignificant for either type I or II fits.

The α values for all the investigated mixtures are negative, indicating that C_p peaks are finite cusps rather than power law singularities. With the exception of the $X = 0{\cdot}106$ mixture, the Fisher-renormalized Ising exponent $\alpha_R = -0{\cdot}124$ lies within the uncertainty of the fitting results. The respective type I fits with α free are shown

together with the ΔC_p data in figure 5. In figures 6(*a*)–(*e*), the type II renormalized Ising fits are shown separately for each sample over the entire fitted temperature range.

3. Discussion

The S_{A_1}–S_{A_2} transition is expected to belong to the 3D Ising universality class [5], but there are complications arising from the coupling of the order parameter to the director fluctuations [8]. The latter feature gives rise to a nonuniversal susceptibility exponent γ that depends on the values of the elastic moduli, but the heat capacity exponent should not be affected. The critical exponent α and amplitude ratio for an Ising transition are $\alpha_I = 0{\cdot}11$ [9] and $A^-/A^+ = 1{\cdot}85$ [15], which are in disagreement with our results.

Since the Fisher renormalized Ising exponent α_R is $-0{\cdot}124$, one explanation of negative α values would be a steep S_{A_1}–S_{A_2} phase boundary dT_c/dX, which can lead to Fisher renormalization [11]. In the case of DB_6CN + TBBA mixtures, $dT_c/dX \simeq -163$ K and Fisher renormalization has been used to explain the observed critical exponents [3, 7]. In the present system, the slopes dT_c/dX range from -110 K to -345 K, as shown in table 1. These values are large enough to produce Fisher renormalization, and our results for all the mixtures with the exception of $X = 0{\cdot}106$ are nicely explained in terms of this idea.

There remains the puzzling question of why the results for the $X = 0{\cdot}106$ mixture are not consistent with the Fisher renormalized α_R value. Two explanations for this seem possible. First, the proximity of the S_{A_1}–S_{A_2} transition to the N–S_{A_1} transition for this mixture makes it difficult to choose the correct $C_p(N\text{–}A_1)$ baseline. Indeed, fits where a term $E_c(T - T_c)$ was included in equation (4) resulted in α values of approximately $-0{\cdot}1$, but the resulting slope E_c had unreasonably large values. Second, it is possible that only partial Fisher renormalization occurs for this sample and an effective exponent α_{eff} is obtained, for which one would expect $-0{\cdot}124 < \alpha_{eff} < 0{\cdot}11$. There is, however, a difficulty with this explanation. The slope dT_c/dX for the $X = 0{\cdot}106$ mixture is almost as large as those for all the other mixtures and is also quite comparable to those in other systems [16] where complete Fisher renormalization takes place.

It should be noted that a tricritical point is expected on the S_{A_1}–S_{A_2} transition line near the N–S_{A_1} critical endpoint at $X^* = 0{\cdot}092$. The α value for the $X = 0{\cdot}106$ mixture is far from the tricritical value $\alpha_t = 1/2$ or its Fisher renormalized version $\alpha_R = -1$. Although a trend may be observed in the free values of the exponent α for the $0{\cdot}106 \leqslant X \leqslant 0{\cdot}163$ mixtures, where α varies from $-0{\cdot}032$ to $-0{\cdot}205$, respectively, this trend is totally unrelated to a possible tricritical Ising-like crossover. If a tricritical point exists between $X = 0{\cdot}092$ and $X = 0{\cdot}106$, the crossover effect must be unusually rapid.

Greater efforts were not made to locate the S_{A_1}–S_{A_2} tricritical point for several reasons: (1) The supply of DB_5CN was limited. (2) It would be difficult to investigate mixtures with $X^* < X < 0{\cdot}106$ since the N–S_{A_1} and S_{A_1}–S_{A_2} peaks would overlap extensively, preventing a critical analysis of α_{eff} for the S_{A_1}–S_{A_2} peak. (3) The shape and magnitude of the S_{A_2} heat capacity 'wing' for the $X = 0{\cdot}087$ sample agree very well with those for the $X = 0{\cdot}106$ sample; compare figures 2 and 3. Thus it seems likely that the S_{A_1}–S_{A_2} behaviour in the range $X^* < X < 0{\cdot}106$ must be very similar to that observed at $X = 0{\cdot}106$.

As shown in table 1, the integrated S_{A_1}–S_{A_2} enthalpy $\delta H = \int \Delta C_p(A_1-A_2)\,dT$ decreases rapidly as X increases, especially for $X > 0{\cdot}134$. In terms of two-scale-factor universality, one would expect $A\xi_0^3$ (where A is the C_p amplitude and ξ_0 is the correlation coefficient in $\xi = \xi_0 t^{-\nu}$) to have a universal value along the S_{A_1}–S_{A_2} line [17]. This implies that ξ_0 should increase appreciably as X increases, a trend that has been observed in DB_6CN + TBBA mixtures [3]. An X-ray study of S_{A_2} critical susceptibility and correlation length behaviour in DB_5CN + TBBA as a function of X would be valuable as a clarification and confirmation of the critical heat capacity trends reported here.

Finally, the critical N–S_{A_1} heat capacity is compatible with 3D-XY behaviour, as expected from recent high-resolution investigations of other polar liquid crystal systems [14]. The N–S_{A_1} transition is difficult to study in DB_5CN + TBBA due to drifts in T_{NA_1} and changes in the N–S_{A_1} peak shape with time. The lower stability near the N–S_{A_1} transition as compared to the S_{A_1}–S_{A_2} transition region is also seen in DB_6CN + TBBA mixtures [3, 7]. As in many other systems, this poor stability is associated more with being in the N phase than with the higher absolute temperature *per se*. For example, TBBA is quite stable at its S_A–S_C transition, which occurs at 445 K [18].

This work was supported by National Science Foundation grant DMR-87-02052 and U.S.–France Cooperative Science grant INT-85-14185.

References

[1] Hardouin, F., Levelut, A. M., Achard, M. F., and Sigaud, G., 1983, *J. Chim. phys.*, **80**, 53, and references cited therein.

[2] Sigaud, G., Hardouin, F., Achard, M. F., and Gasparoux, H., 1979, *J. Phys., Paris*, **40**, C3-356. Sigaud, G., Hardouin, F., and Achard, M. F., 1979, *Physics Lett.* A, **72**, 24.

[3] Chan, K. K., Pershan, P. S., Sorensen, L. B., and Hardouin, F., 1985, *Phys. Rev. Lett.*, **54**, 1694; 1986, *Phys. Rev.* A, **34**, 1420.

[4] Levelut, A. M., 1984, *J. Phys. Lett., Paris*, **45**, L603. Sigaud, G., Achard, M. F., and Hardouin, F., 1985, *J. Phys. Lett., Paris*, **46**, L825.

[5] Prost, J., 1979, *J. Phys., Paris*, **40**, 581; 1980, *Liquid Crystals of One- and Two-Dimensional Order* (Springer Series in Chemical Physics, Vol. 11) (Springer-Verlag), p. 125; 1984, *Adv. Phys.*, **33**, 1.

[6] Hardouin, F., Levelut, A. M., Benattar, J. J., and Sigaud, G., 1980, *Solid St. Commun.*, **33**, 337. Hardouin, F., Levelut, A. M., and Sigaud, G., 1981, *J. Phys., Paris*, **42**, 107.

[7] Garland, C. W., Chiang, C., and Hardouin, F., 1986, *Liq. Crystals*, **1**, 81.

[8] Wang, J., and Lubensky, T. C., 1984, *Phys. Rev.* A, **29**, 2210.

[9] LeGuillon, J. C., and Zinn-Justin, J., 1977, *Phys. Rev. Lett.*, **39**, 95; 1980, *Phys. Rev.* B, **21**, 3976.

[10] Fisher, M. E., 1968, *Phys. Rev.*, **176**, 257. Fisher, M. E., and Scesney, P. E., 1970, *Phys. Rev.* A, **2**, 825.

[11] Huse, D. A., 1985, *Phys. Rev. Lett.*, **55**, 2228.

[12] Anisimov, M. A., Voronel, A. V., and Gorodetskii, E. E., 1971, *Sov. Phys. JETP*, **33**, 605.

[13] Garland, C. W., 1985, *Thermochim. Acta*, **88**, 127.

[14] Garland, C. W., Nounesis, G., and Stine, K. J., 1989, *Phys. Rev.* A, **39**, 4919.

[15] Bagnuls, C., Bervillier, C., Meiron, D. I., and Nickel, B. G., 1987, *Phys. Rev.* B, **35**, 3585.

[16] Huster, M. E., Stine, K. J., and Garland, C. W., 1987, *Phys. Rev.* A, **36**, 2364.

[17] Sanchez, G., Meichle, M., and Garland, C. W., 1983, *Phys. Rev.* A, **28**, 1647, and references cited therein.

[18] Das, P., Ema, K., and Garland, C. W., 1989, *Liq. Crystals*, **4**, 205.